The flow of AAIW along the equator

M. Jochum * and P. Malanotte-Rizzoli

in: Interhemispheric Water Exchange in the Atlanic Ocean
Elsevier Series, p 193-212

A numerical model of the Atlantic ocean is used to understand the observations of the Antarctic Intermediate Water (AAIW) along the equatorial Atlantic. It is demonstrated that the the available velocity measurements of the equatorial AAIW can be explained by seasonal Rossby waves, and that their previous interpretation as strong zonal currents could be the result of an aliasing of the tropical wave field. Although this model study suggests that there is no Eulerian mean flow of AAIW along the equator, it shows that planetary waves induce a zonal Stokes drift.

1. INTRODUCTION

Antarctic Intermediate Water (AAIW) spreads from the subantarctic region to the northern hemisphere in all three oceans. Recently, its circulation in the Atlantic received much attention because it is thought to provide a substantial part of the return flow of the Meridional Overturning Circulation (MOC, *Rintoul*, 1991). This buoyancy-driven global circulation is responsible for a substantial part of the northward heat flux in the Atlantic ocean. Despite the importance of the Atlantic AAIW, its circulation patterns and strength are poorly constrained by observations. Especially the tropics with their strong variability are undersampled (see *Suga and Talley*, 1995 for a recent analysis).

The origins and pathways by which the AAIW enters the South Atlantic are still unclear. However, at approximately $10°$S it appears to flow north in an Intermediate Western Boundary Current (IWBC). The water is characterized by a salinity minimum and a local oxygen maximum which have their depths in the tropics at approximately 700 m. *Suga and Talley* (1995) show that the AAIW is confined to the western boundary except for a long tongue that reaches east at $4°$S. Two recent zonal hydrographic sections by *Arhan et al.* (1998) indicate that the AAIW enters the equatorial region at $4.5°$S in an IWBC and no AAIW crosses the $7.5°$N section in the interior. Various investigators estimated with different

*Corresponding author. Tel.: +1-617-253-3573. *Email address:* markus@ocean.mit.edu

methods that between 5 Sv and 10 Sv of AAIW flow from the southern into the northern hemisphere (*Roemmich*, 1983, *Schmitz and Richardson*, 1991, *Schott et al.*, 1998).

It is less clear how the AAIW crosses or spreads along the equator. Based on four meridional LADCP-sections across the equator *Schott et al.* (1998) claim the existence of strong zonal currents along the equator which could explain the equatorial tracer tongue. OGCM studies of the tropical circulation, however, could not reproduce these intermediate currents which was commonly seen as a deficiency of the model (*Boening and Schott*, 1993, *Blanke et al.*, 1999). However, a dynamical explanation for the observed intermediate currents has not yet been provided.

This chapter describes experiments with a numerical model that offer new interpretations of the velocity observations at intermediate depth along the equator. It is structured as follows: first, the numerical model and the performed experiments are described, and the model results will be shown to be consistent with the available observations of the equatorial AAIW. Second, the dynamics of the AAIW flow along the equator is investigated. Results are summarized in Section 4.

2. THE MODEL CONFIGURATION

The model used is the MOM2b code and the setup allows for the investigation of the intermediate flow, although it was initially designed to study the generation of North Brazil Current rings. This explains some of the particular choices that were made for the spatial resolution and the boundary conditions.

The domain is an idealized basin from $25°$S to $30°$N in latitude and from $70°$W to $15°$E in longitude, with a flat bottom at 3000 m. The resolution is $1/4°$ by $1/4°$ at the western boundary between the equator and $12°$N and becomes coarser towards the eastern, northern and southern boundaries: the latitudinal resolution is reduced from $1/4°$ to $1°$ at the meridional boundaries; the longitudinal resolution is reduced from $1/4°$ to $1.5°$ at the zonal boundaries (see Figure 1 for an illustration of the resolution). There are 30 levels in the vertical with a 10 m resolution in the top 100 m.

The horizontal mixing is done by a Laplacian scheme with the eddy viscosity and diffusivity being linearly dependent on the resolution: from $200\ \mathrm{m}^2/\mathrm{s}$ for $1/4°$ to $2000\ \mathrm{m}^2/\mathrm{s}$ for $1°$ resolution. In the vertical, a Richardson number-dependent vertical mixing scheme is used. Unstable temperature gradients are eliminated by mixing heat vertically to a depth that ensures a stable density gradient.

The initial condition is a state of rest. Salinity remains a constant value of 35 psu. The wind stress (*Hellerman and Rosenstein*, 1983) and the resulting depth integrated circulation are shown in Figures 1 and 2. The initial temperature is prescribed as shown in Figure 1 of *Liu and Philander* (1995). This profile is also used at the surface to restore the surface temperature with a 40-day relaxation time. The experiment was integrated for 20 years before any analysis

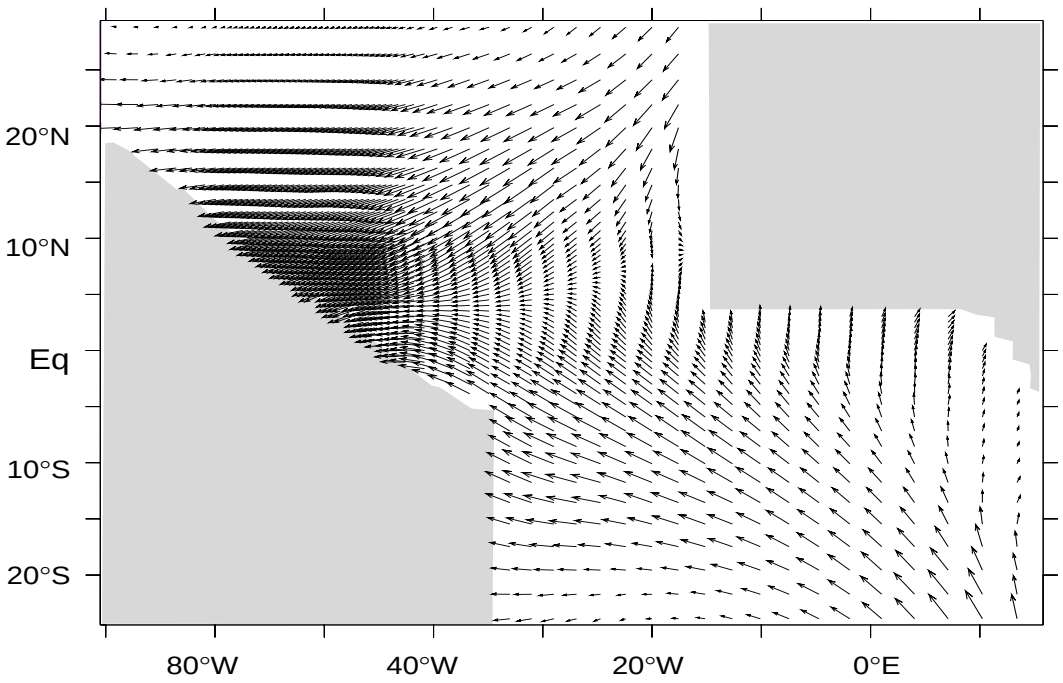

Figure 1: The annual mean wind stress over the domain where for the sake of clarity only every fourth gridpoint is shown. The Caribbean Sea is not part of the model domain.

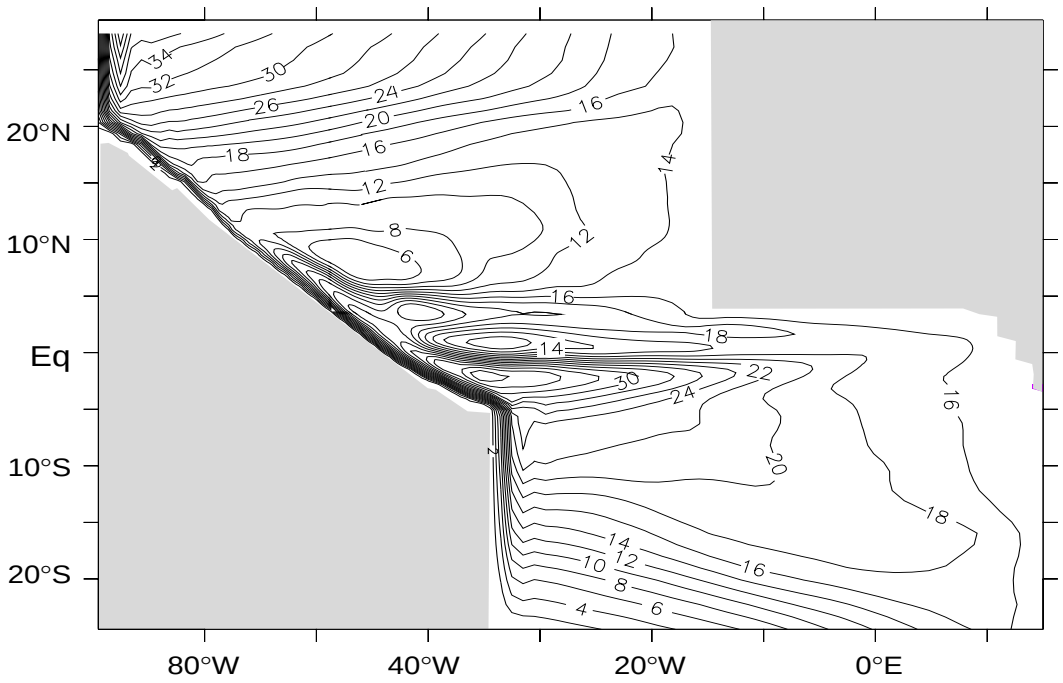

Figure 2: The time mean depth integrated transport (in Sv). The water enters the domain along the northern and southern open boundary and leaves it again through the northern open boundary in the Gulf Stream.

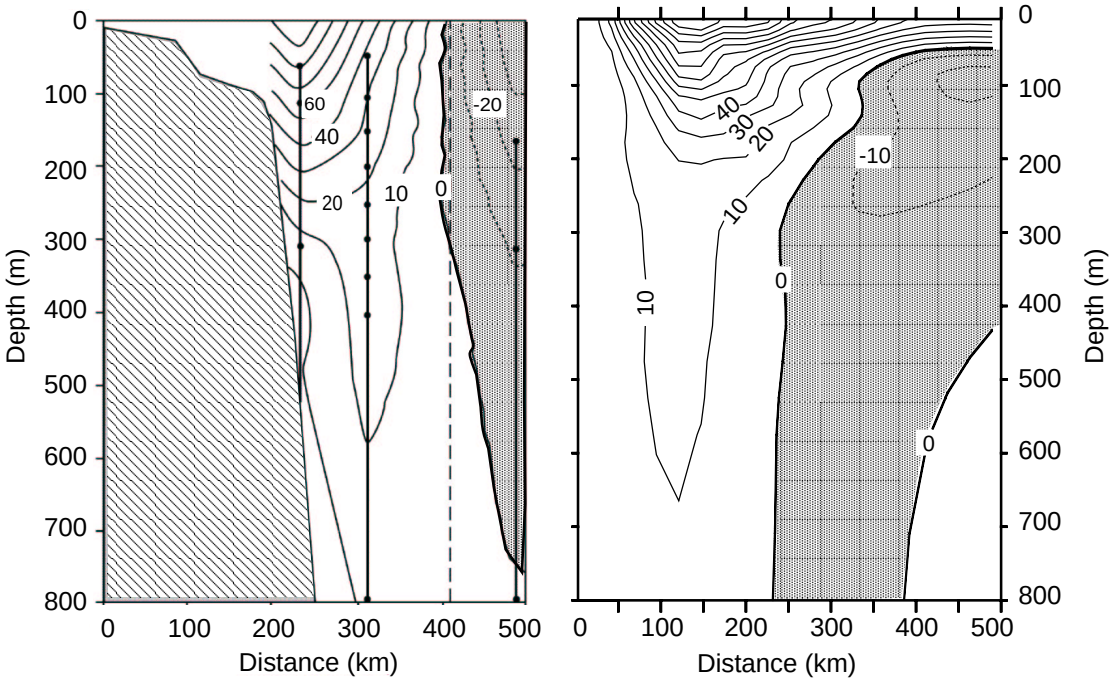

Figure 3: (left) The alongshore velocity (in cm/s) at 4°N averaged over 16 months modified from *Johns et al.* (1998); (right) as obtained in the model for the same period.

was performed (for a justification, see *Liu and Philander*, 1995). The mean fields, which will be referred to later in the text, are the result of a four year average.

The effect of the global MOC was represented by open boundary conditions (OBC). It is known that OBC render the problem of solving the primitive equations ill posed (*Oliger and Sundstrom*, 1978). Nevertheless, progress can be made if the errors that are introduced by the OBC are small enough and do not grow in time (*Spall and Robinson*, 1989).

MOM2b provides subroutines for OBC that were modified for the purposes of this study. At the open boundaries the temperature and the barotropic streamfunction are specified. Using the Sverdrup balance and geostrophy the model calculates the velocity field (*Stevens*, 1990). The barotropic streamfunction and temperature at the meridional boundaries are taken from the steady state solution of the purely wind-driven circulation. The basin for the purely wind-driven circulation extends from 40°S to 40°N. To simulate the throughflow of the MOC return flow, the barotropic streamfunction is modified so that there are 15 Sv flowing into the South Atlantic all along the southern boundary and leaving the North Atlantic in the northwest corner through a western boundary current . These 15 Sv are roughly consistent with numbers from the literature (*Schmitz and McCartney*, 1993) and the Sverdrup transport across 25°S. It was not attempted to simulate a deep western boundary current because emphasis was put on the warm water return flow of the MOC and its interaction with the wind-driven circulation.

To gain confidence in the model results, they were compared with the available observations for the AAIW. Traditionally, the core of the AAIW is determined

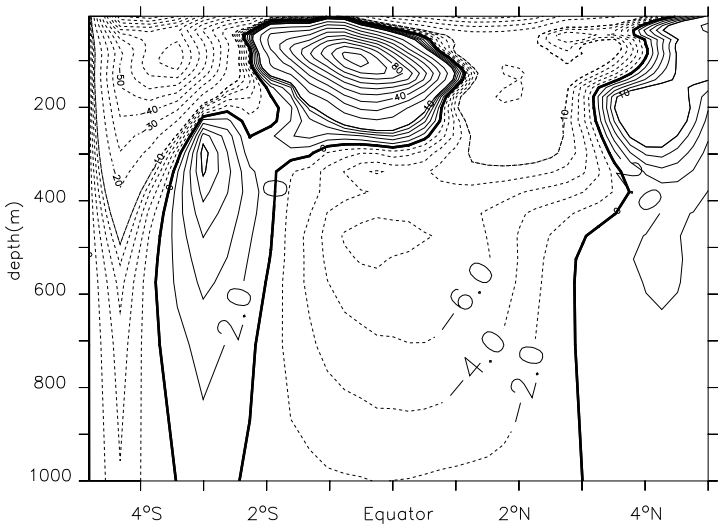

Figure 4: The zonal velocity at $35°$W, averaged using 4 sections taken in the same months as the sections by *Schott et al.*'s (1998). Contours are every 1 cm/s between -10 cm/s and 10cm/s and every 10cm/s for higher velocities.

by the salinity minimum and the oxygen maximum. The exact definition of the AAIW varies with author and region of study, and it encompasses the depth range between 300 m and 1200 m. This model does not feature salinity or oxygen. Therefore, a new water mass is defined and called IW, denoting all the waters between the $5.5°$C and the $13.5°$C isotherms that originate at the southern open boundary. At the equator, this IW is located approximately between 300 m and 1000 m and is represented by 8 model levels. Several factors led to this choice. First, the resolution below 1000 m becomes very coarse (2 layers for 1700 m). Second, the only two authors that made a quantitative estimate of the AAIW flux through the tropics chose as vertical limits 330 m - 870 m (*Roemmich*, 1983) and 300 m - 1000 m (*Schott et al.*, 1998). Our choice makes the comparison between their values and our model results more meaningful.

The model results show that approximately 6 Sv of water flow from the southern to the northern hemisphere (almost entirely along the western boundary), which is within the range of the observed transports. The comparison with the available current meter data is encouraging as well. On crossing the equator, the model IWBC reaches velocities that are similar to observations by *Schott et al.* (1998): the modeled IWBC has an alongshore velocity of 8 +/- 6 cm/s at 850 m depth. *Schott et al.* (1993) measure 5 +/- 19 cm/s at the same location. The lower variability of the model may be due to the absence of topography or to a wind field with an unrealistically low variability. The agreement with mooring data at $4°$N (*Johns et al.*, 1998, see the comparison in Figure 3) is even better.

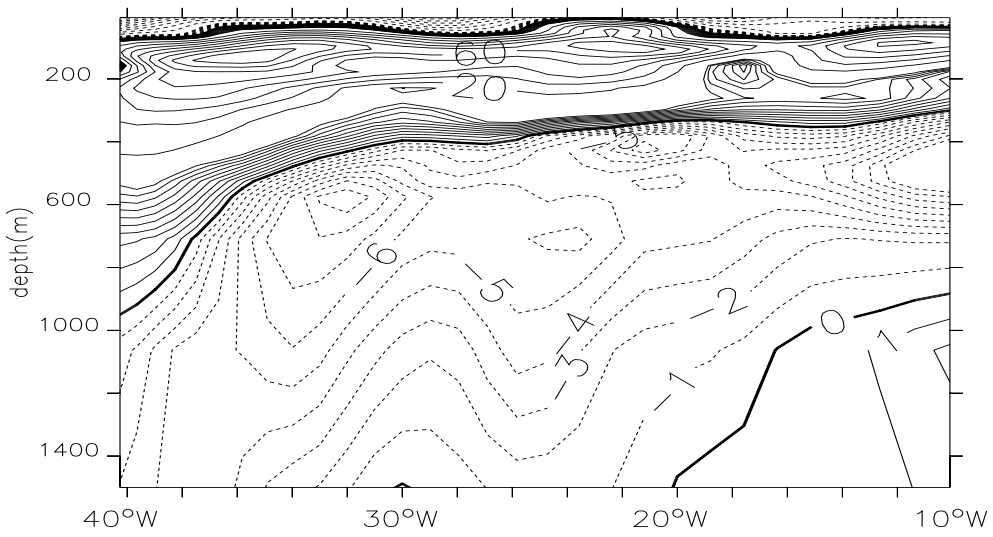

Figure 5: The modeled zonal velocity along the equator in August. The contour lines are every 1 cm/s between -10 cm/s and 10 cm/s and every 10 cm/s beyond.

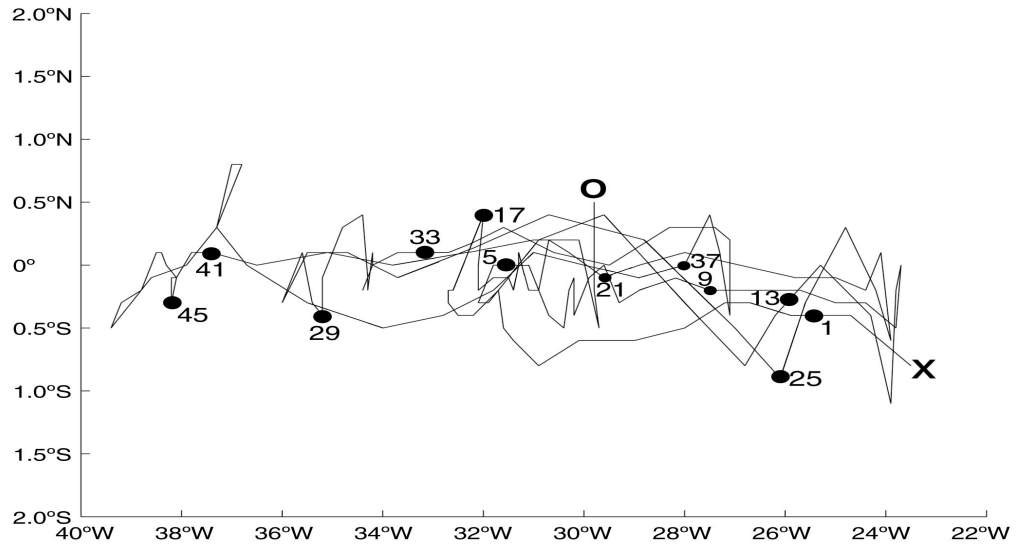

Figure 6: The trajectory of a single virtual particle in the model. Shown is the area between 2°S and 2°N and between 40°W and 22°W. The float is launched at 23°W at 450 m depth (x) and can reach zonal velocities of more than 5 cm/s over a period of several months. The numbers in the pictures denote the time (in months) after launching the float, the circle shows its final position after 4 years.

Lowered Acoustic Doppler Current Profiler (LADCP) measurements along $35°$W are available from *Schott et al.* (1998). The average of 4 sections show at intermediate levels an eastward flow centered at $2.5°$S and $2°$N and a westward flow at the equator. At approximately the same times and locations the model has a similar velocity structure (albeit weaker amplitude) at intermediate depths (compare their Figure 15c with Figure 4). An additional set of LADCP measurements is available from *Schmid et al.* (2001) showing a section of zonal velocity along the equator. These observations were done during the summer and they show essentially a westward flow between 500 m and 1500 m depth and eastward flow between 50 m and 500 m depth (see their Figure 13). The model results show again a striking similarity with the observations (Figure 5).

The available float data shows that the flow is mainly zonal, reverses its direction over the course of a year, and has peak velocities of approximately 20 cm/s (*Richardson and Schmitz*, 1993, *Boebel et al.* 1999a, 1999b, *Ollitrault, pers. comm.* and *Schmid et al.*, 2001). The simulated floats in the model show a similar behavior. Figure 6 shows the typical path of a float in the interior of the equatorial Atlantic at intermediate depths: it covers a large zonal distance before turning around and returning towards its initial longitude. As in the comparison of the Eulerian fields, the float velocities are smaller in the model than in the observations, with their peak velocities being approximately 10 cm/s. This basic comparison with the velocity observations along the equator at intermediate depths is encouraging. A detailed analysis of individual measurements and of the AAIW flow in the model follows in the next section.

3. SYNTHESIS OF THEORY AND OBSERVATIONS

Before trying to understand the observations, the topic of equatorial waves is addressed. Because of the strong changes in the Ekman divergence along the equator and the high wave speed in the tropics, it is expected that every observation in the region will be highly contaminated with waves. One of the advantages of using a General Circulation Model (GCM) is that the structure of these waves can be analyzed to estimate how they may affect the signal of interest. In the equatorial Atlantic the strong stratification leads to the dominance of the second baroclinic mode (*Philander*, 1990). This is different from the Pacific, which has a much deeper thermocline and therefore projects most of its seasonal variability on the first baroclinic mode (compare *Busalacchi and O'Brien*, 1980 with *Busalacchi and Picault*, 1983). The reason for this difference is not clear; however, a comparative study of the Pacific and the Atlantic is beyond the scope of our work. Figures 7 and 8 display the model's first and second Empirical Orthogonal Function (EOF) of the zonal velocity at $35°$W. The first EOF is much stronger than the second, and its equatorial zero crossings at 2200 m and 650 m illustrate the dominance of the second baroclinc mode, comparing well with the theoretical predictions of 2200 m and 500 m which was computed by *Philander* (1990) for the stratification of the model. The sidelobes at $5°$S and $5°$N are a part of

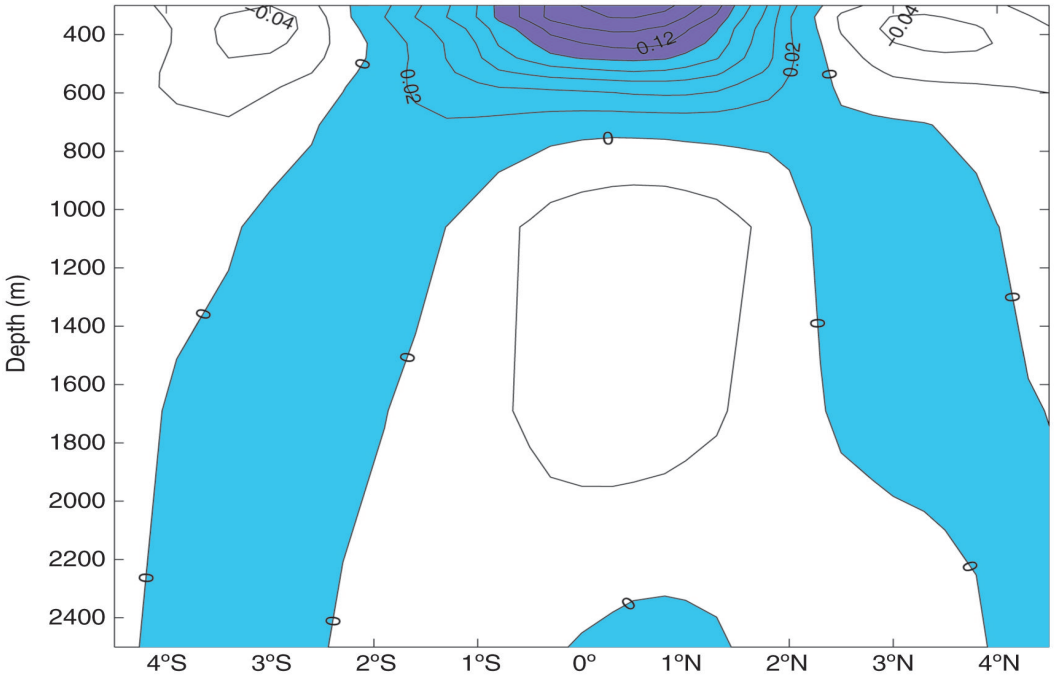

Figure 7: The first EOF of the zonal velocity at 35°W, positive values are shaded. Only the flow below the thermocline (300m) is considered because the upper layer flow is governed by different dynamics. This mode explains 56% of the variability.

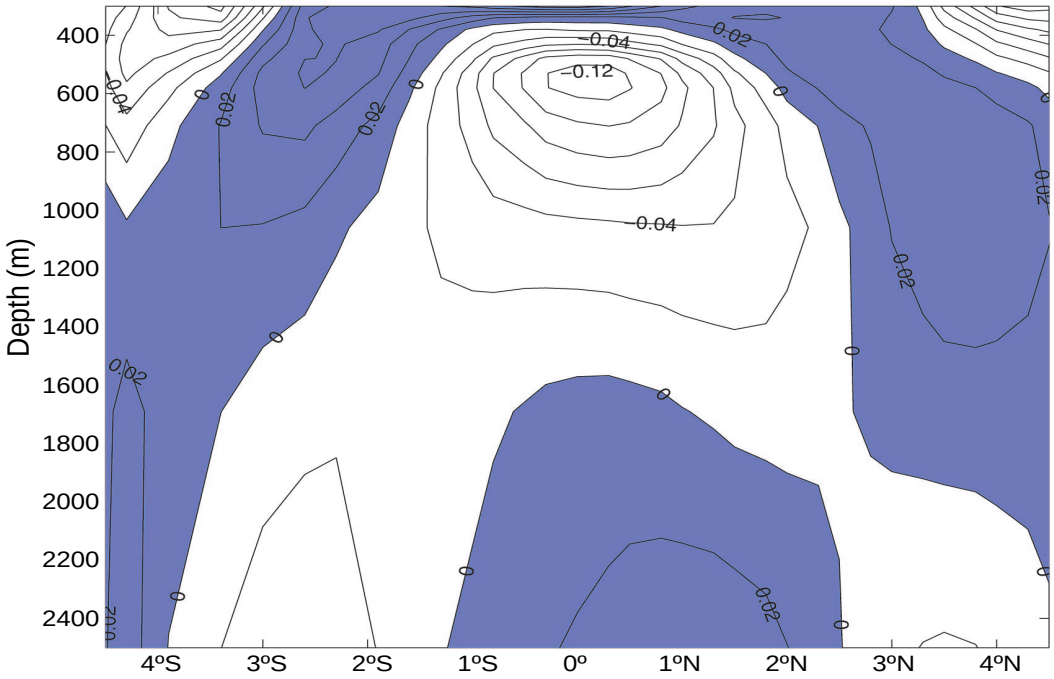

Figure 8: The second EOF of the zonal velocity at 35°W, positive values are shaded. This mode explains 15% of the variability.

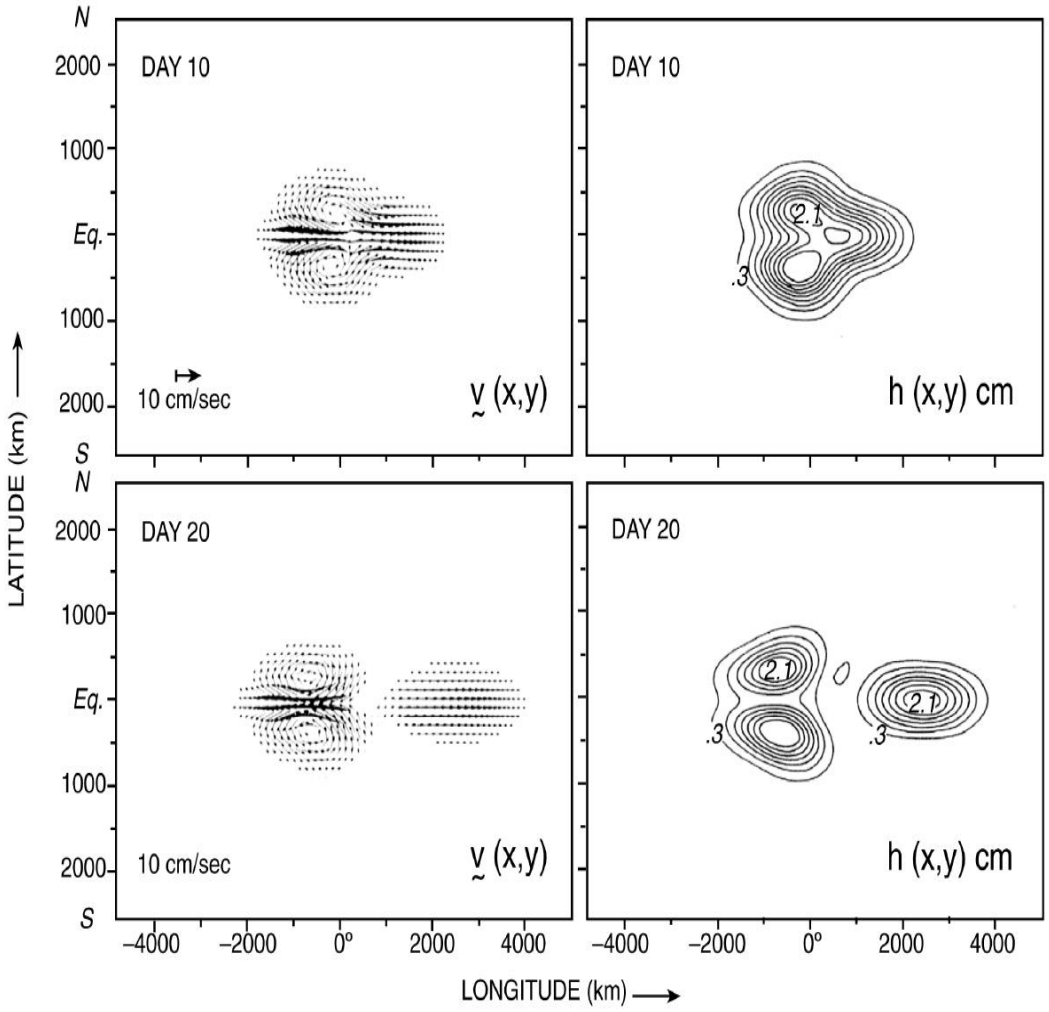

Figure 9: Current velocity and sea surface high anomaly caused by an initial Gaussian sea surface height disturbance at the equator (adapted from *Philander et al.*, 1984).

the Rossby wave and can best be understood with the help of Figure 9: the seasonal wind field variation causes an Ekman convergence which translates into a SSH anomaly (in Philander's barotropic model). This height anomaly projects on a set of Kelvin and Rossby waves. The Rossby waves are an essential part of this set because the Kelvin wave does not have a signal outside the equatorial deformation radius. Thus, the sidelobes seen in the EOF (Figures 8 and 9) are the result of the same two pressure anomalies that cause the strong velocity peak at the equator. The theoretical structure of the zonal velocity of the first two symmetrical and the first antisymmetrical meridional Rossby modes are shown in Figure 10. A comparison with the EOFs at intermediate depth suggest that the first EOF reflects the first symmetric mode, while the second EOF reflects the second symmetric meridional Rossby wave mode. The relative strengths of the modes depends on the spatial structure of the wind field variability that projects on these modes. The

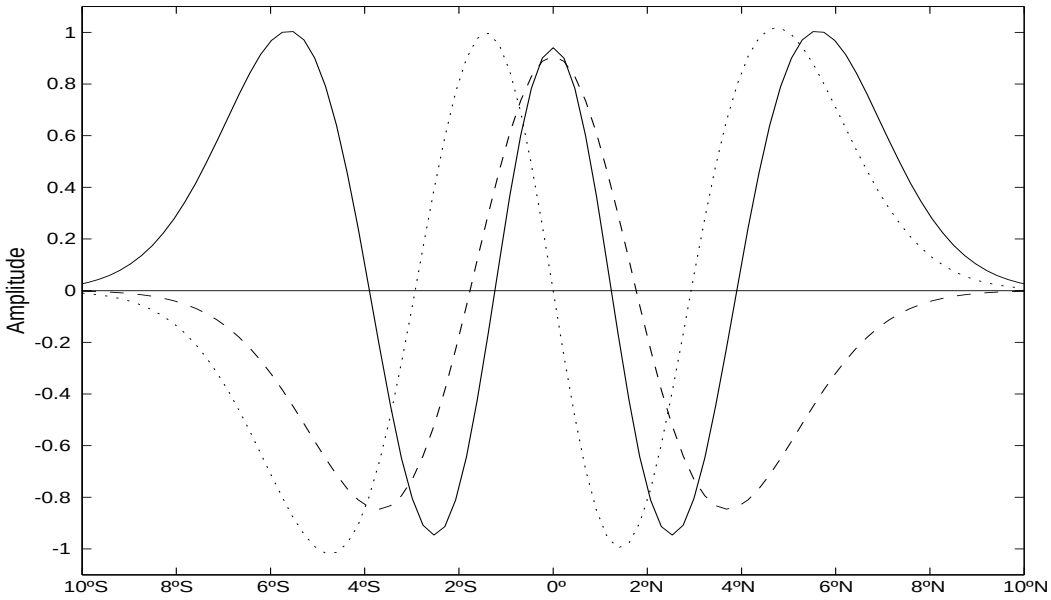

Figure 10: The meridional structure of the first (dashed line) and second (solid line) symmetrical mode of the zonal velocities of equatorial Rossby waves. The structure of the first antisymmetrical mode is indicated with dots.

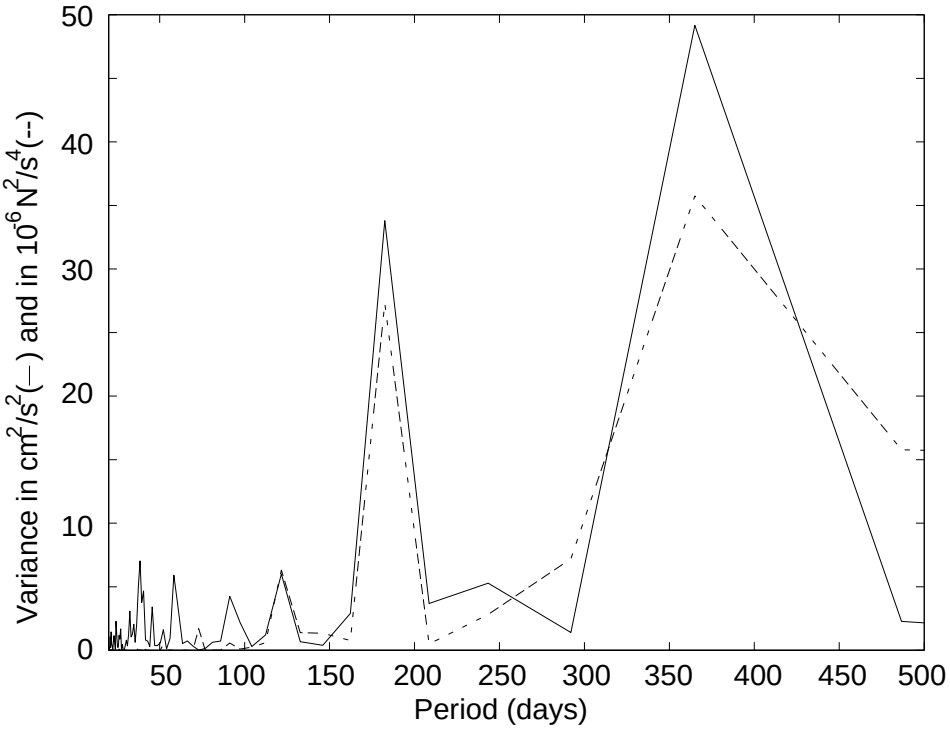

Figure 11: Variance conserving spectrum of the zonal velocity at $25°$W/$0°$N at 500m depth (solid line, peak at 50 cm^2/s^2), and the spectrum of the zonal wind stress at the same position (dashed line, in 10^{-6} N^2/s^4).

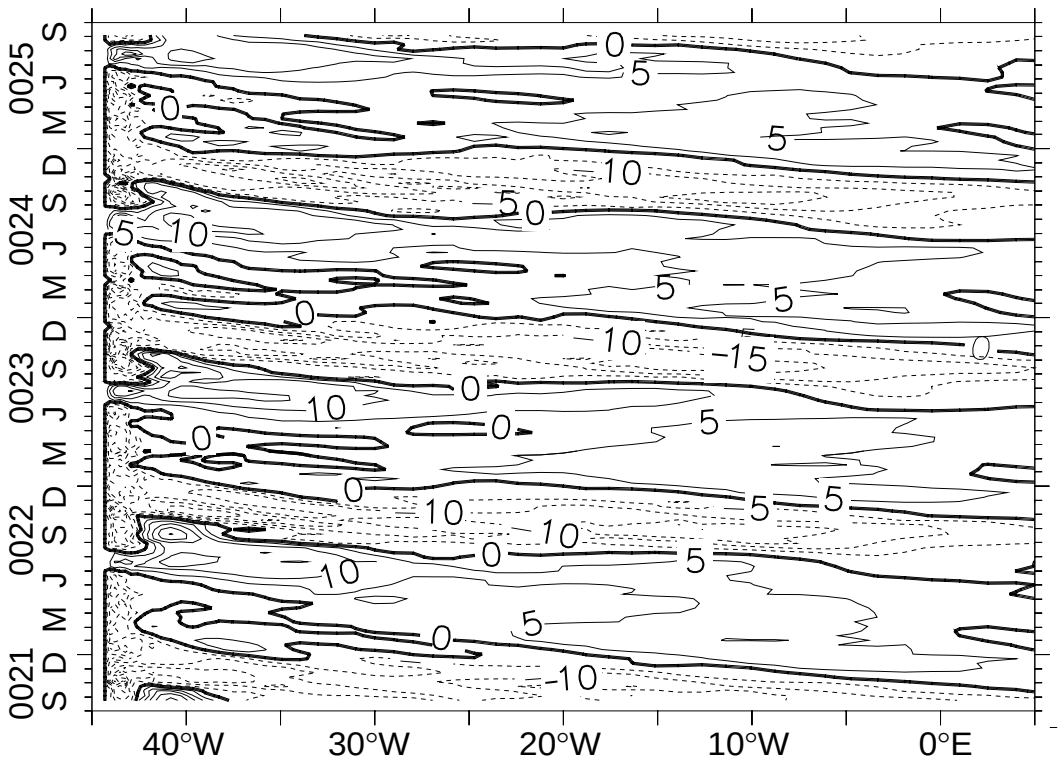

Figure 12: Space-time diagram for the zonal velocity along the equator at 500 m depth (cm/s) for years 21 through 25. Contours are every 5cm/s.

corresponding Kelvin wave could not be detected in the model solution because its phase speed is more than 1 m/s and the model results are only stored every 10 days. The Rossby waves are excited by the annual and semiannual wind field variations (Figure 11) and have the following dispersion relation (*Philander*, 1990):

$$\sigma = -\beta\lambda^2 k/3 \ ,$$

where k is the zonal wave number, $\beta = 2.3 \cdot 10^{-11}(\mathrm{ms})^{-1}$, and $\lambda = 250$ km is the Rossby radius of the second baroclinic mode. From this, a Rossby wave with yearly forcing is expected to have a wavelength of 15000 km and a phase speed of 0.47 m/s. Figure 12 shows that the waves seen in the model have a wavelength of more than twice the basin width (= 6000 km) and phase speed of approximately 0.4 m/s. Thus, below the thermocline the equatorial flow field is dominated by seasonal Rossby waves of the second baroclinic mode.

Water properties and floats are not advected by the time mean flow but instead by the turbulent flow, making the interpretation of observations much more complicated, especially in the presence of strong planetary waves. As an example, Figure 13 shows the path of a virtual float at 500 m depth. Although there is almost no mean eastward flow (Figure 14), the final position of this float is 1000 km east of the western boundary.

After this introduction, we can now turn to the interpretation of the obser-

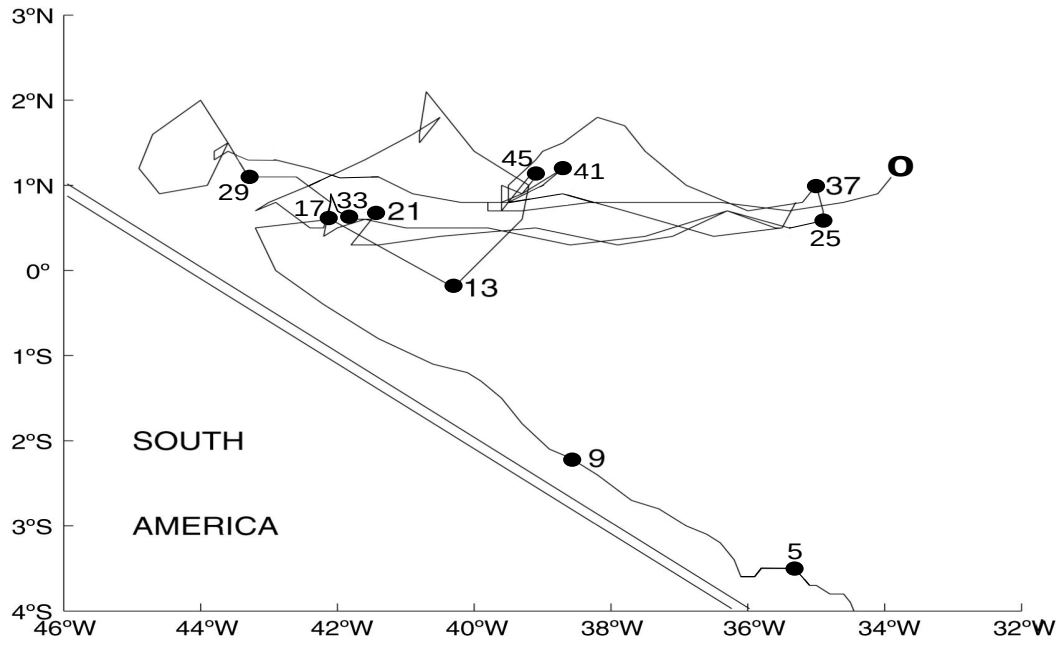

Figure 13: The pathway of a virtual float at 500 m depth. The float was launched in the IWBC at 8°S, and its final position after 4 years is marked with a circle. The numbers indicate the months after launch.

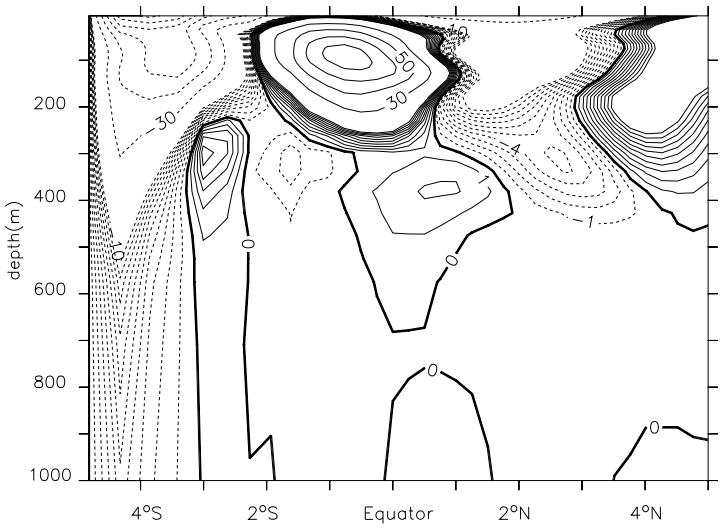

Figure 14: The 4 year mean of the zonal velocity across the equator at 35°W. The contour interval is 1 cm/s between -10 cm/s and 10 cm/s and every 20 cm/s beyond.

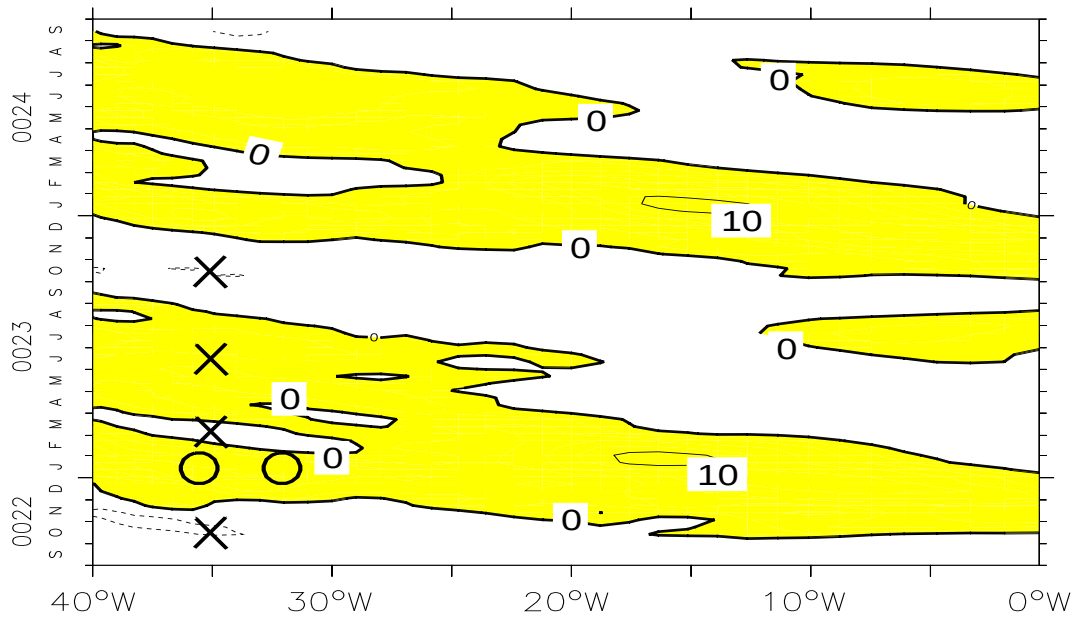

Figure 15: Space-time diagram of the zonal velocity at 700 m depth. The eastward velocity is shaded, the contour intervals are 10 cm/s. The crosses indicate the time and position of the *Schott et al.* (1998) measurements and the circles show the launching time and position of the two *Richardson and Schmitz* (1993) SOFAR floats that were released away from the western boundary.

vations introduced in section two. The initial motivation for this research is the observation of bands of strong zonal velocities at intermediate depths found by *Schott et al.* (1998). They interpreted these observations as strong zonal currents, although their existence defied any explanation and contradicts the float observations by *Richardson and Schmitz* (1993). Strangely, this has not received any attention in the literature. In fact, model studies interpret the lack of strong intermediate currents as a deficiency of the model (*Boening and Schott*, 1993; *Blanke et al.*, 1999). The comparison of Figure 15c of *Schott et al.* (1998) with Figure 4 shows that the present model is able to reproduce the observed spatial structure of the observations (the amplitude, however, is too small). The model also shows that there is no zonal flow in the yearly mean (Figure 14). This suggests that the interpretation of the observations by *Schott et al.* (1998) can be explained by aliasing of the tropical wave field. Figure 15 shows a space-time diagram of the zonal velocity at intermediate depths, where the time and locations of the available measurements are indicated by crosses and circles. This diagram illustrates that all six observations (4 ADCP sections and 2 float trajectories) can be explained by seasonal Rossby waves. The model predicts eastward flow for the two floats in January, strong westward flow in October, weak westward flow in March and weak eastward flow in June. Given the uncertainties in the wind field, the comparison with the observations is strikingly good.

There are, however, differences between the observations and the model results. Figure 16 shows snapshots of zonal velocity from the model output, which

can be compared directly with the observations (see Figure 14 of *Schott et al.*, 1998). Ideally, one would project a long time series of zonal velocity on the different possible equatorial modes and compare their amplitude in the model with the ones in the observations. Unfortunately, this is not possible because of the few number of observations. Furthermore, the zonal velocities of the different equatorial modes are not linearly independent. Therefore, one can only qualitatively compare the observations with the model snapshots. The October snapshots and the October observations compare well with the predicted structure of the first

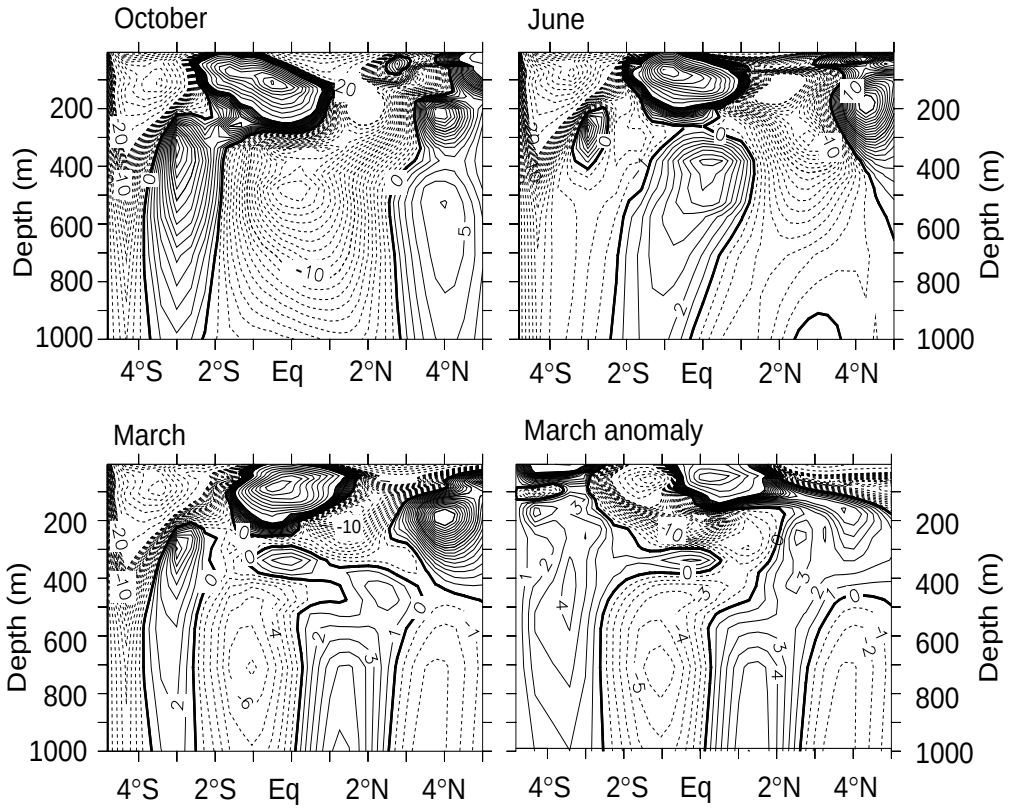

Figure 16: The zonal velocity across 35°W as computed in the model. The counter interval is 1 cm/s between -20cm/s and 20cm/s and 10 cm/s beyond. Comparison with Figure 14 of *Schott et al.* (1998) and Figure 10 shows that October (upper left) is dominated by a Rossby wave of the first symmetrical mode in the model and in the observations. The June (upper right) snapshot is difficult to interpret and the March velocity anomalies (lower right) suggest that March (lower left) is dominated by the first antisymmetrical mode (see Figure 10).

symmetrical mode (Figure 10). The March observations are reminiscent of the second symmetrical mode, whereas the model's velocity field looks more like the first antisymmetrical mode (Figure 10). The observations and the model results for June are difficult to interpret as a single mode, as they are likely to be the superposition of different modes.

While the model is not able to reproduce every single velocity section, it correctly predicts the phase and the strength of the first symmetric mode, which in the model accounts for 56% of the variability and in the observations produces the strongest transports. The model furthermore predicts correctly the eastward flow in late January. The higher latitudinal modes are apparently not reproduced correctly which might be due to an unrealistic stratification or a possibly unrealistic wind field used in the model. It is conceivable that the real wind, which excites the

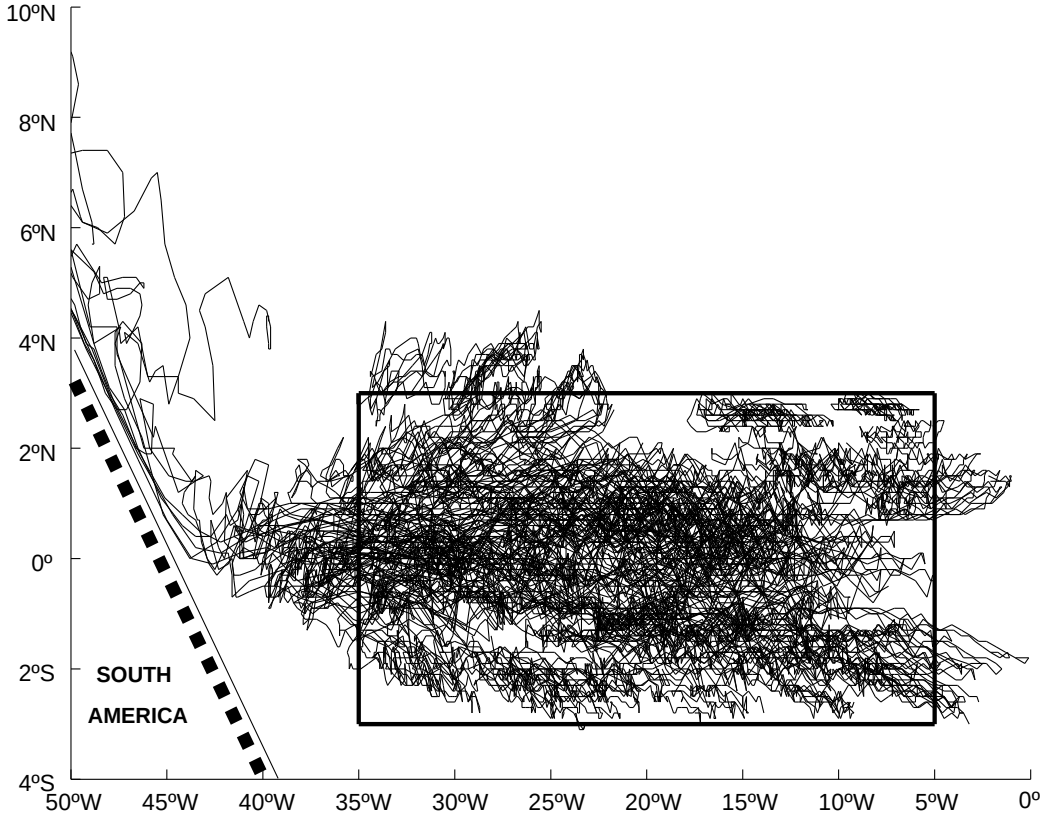

Figure 17: The trajectories of floats that were released in the box at 450 m depth. After 4 years, the easterly tongues polewards of the equator and the westerly tongue on the equator can be observed.

waves in the ocean, has a different structure than the Hellerman-Rosenstein wind field used in the model and, therefore, projects differently on the higher modes than the model winds.

The LADCP observations by *Schott et al.* (1998) are discussed here in great detail, because they are commonly used to support the claim of strong zonal jets. The discussion above showed that these observations could be interpreted

alternatively as seasonal Rossby waves. Other known observations at intermediate depth are consistent with this wave interpretation and they are listed below:

- With a one year current meter deployment at $0°$N/$4°$W, *Weisberg and Horigan* (1981) observe that the zonal velocity at 870 m oscillates around an unspecified mean value. The mean has not been specified because the data time scales are similar to the record lengths.
- Based on the trajectories of several PALACE floats, *Schmid at al.* (2001) show that there is no significant mean flow at $6°$S or between $2°$N and $6°$N at 1000 m depth. In the same study they show that there is a westward flow during the summer along the equator at 1000 m depth. This compares well with the phase of the dominant seasonal wave in the model (Figure 5).
- During the Global Atmosphere and Tropical Ocean Experiment (GATE), using a 30 day mooring deployment in August, *Weisberg* (1980) observes a westward flow along the equator at $10°$W at 700 m depth - again well reproduced in the model (Figure 5). In the same season, *Weisberg et al.* (1980) find no significant mean flow at $28°$W/$1.5°$N in 1050 m depth.

While the present analysis does cast doubt on the existence of strong zonal currents, there is the possibility that the waves generate a weak mean flow along the equator. The remainder of this chapter will investigate this mean flow. For this purpose, 100 floats were released in the equatorial waveguide at 450 m depth (Figure 17), and the flow properties of the AAIW layer were computed by analyzing the velocity statistics of the floats. This was motivated by a study of *Li et al.* (1996), who found that in the equatorial waveguide below the thermocline

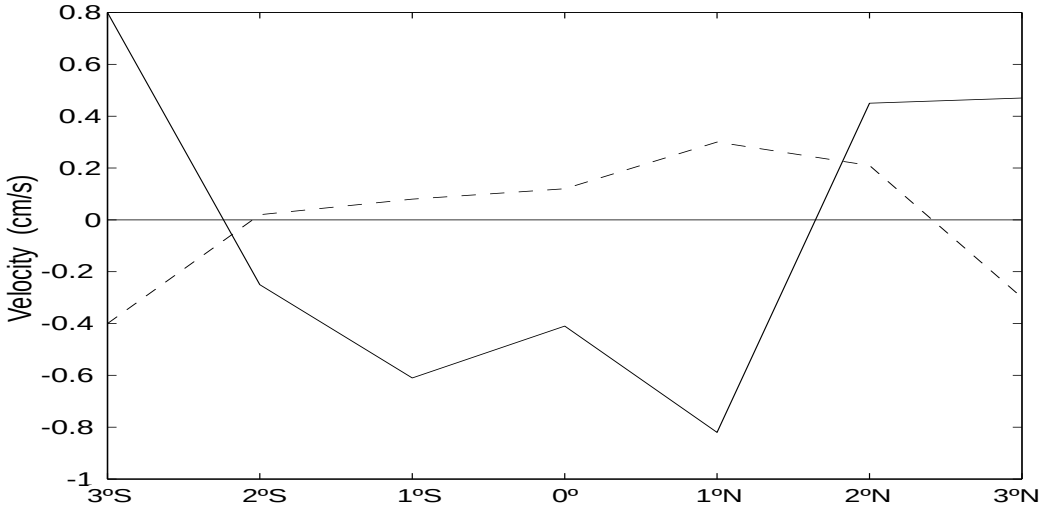

Figure 18: The zonally averaged Lagrangian mean zonal velocity (solid line) and Eulerian mean zonal velocity (broken line) at 450 m depth (in cm/s). The uncertainty of the mean is less than 0.06 cm/s everywhere.

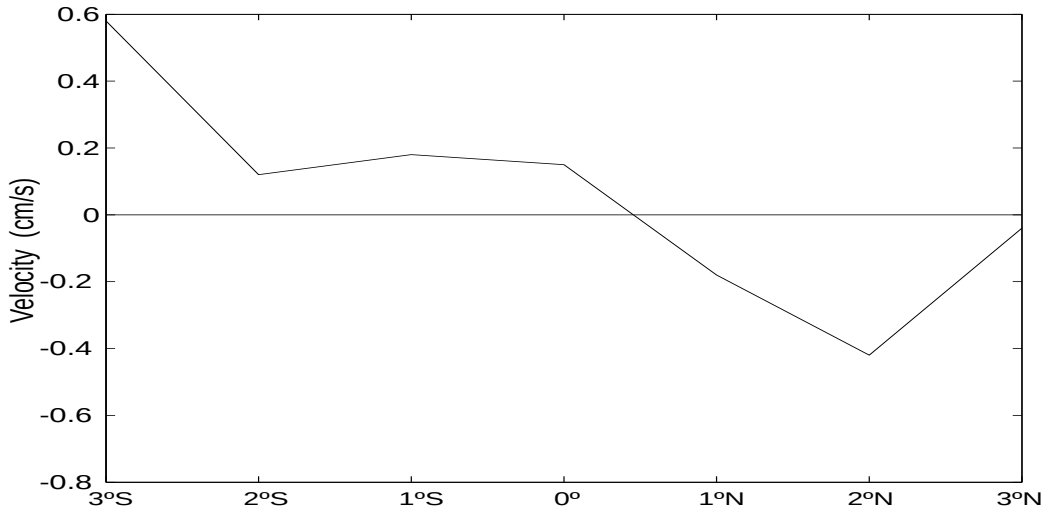

Figure 19: The zonally averaged Lagrangian mean meridional velocity at 450m depth (in cm/s). The Eulerian mean velocity is not significantly different from zero. The uncertainty for the Lagrangian mean is less than 0.015 cm/s, everywhere except for the flow at 3°S where it is 0.05 cm/s.

the Eulerian mean flow is very different from the Lagrangian mean flow. Instead, the Stokes drift that is induced by the seasonal Rossby waves dominates the flow and is of a sign opposite to that of the mean. This can be observed in the present solution too. The trajectories of the released floats are shown in Figure 17. A net eastward displacement polewards of the equator and a net westward displacement

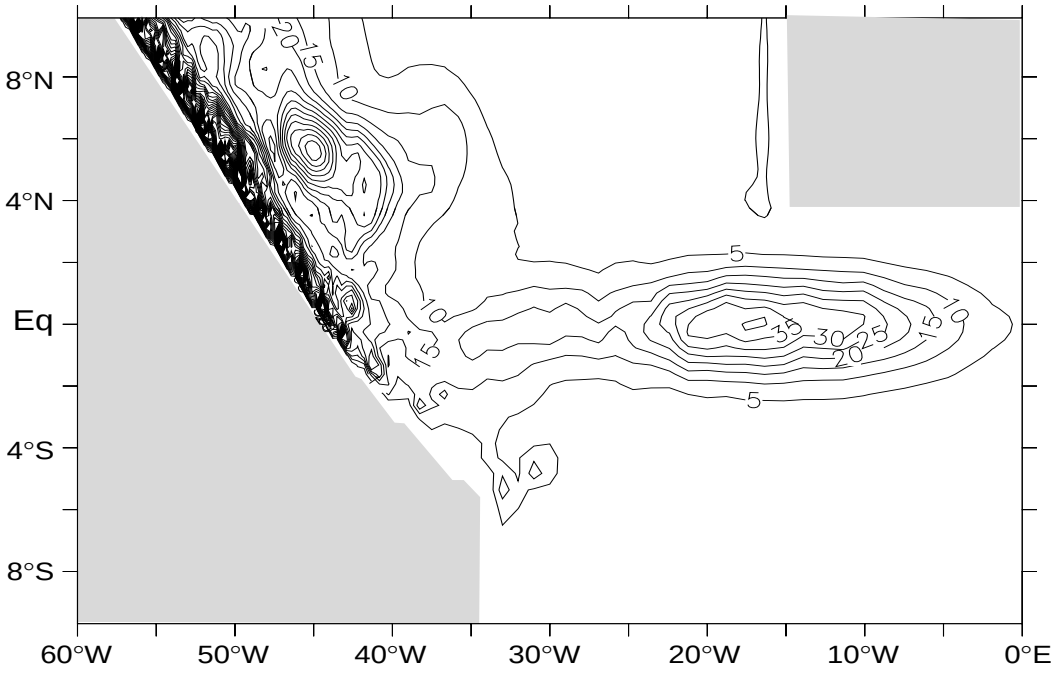

Figure 20: The variance of the meridional velocity at 450 m depth in cm^2/s^2.

on the equator can be seen. To be more quantitative, the area between 36°W and 0°W, and between 3°S and 3°N was partitioned into 1°x1° boxes and the Lagrangian mean velocity was computed in each of these boxes. Figure 18 shows the zonally averaged Eulerian mean flow and the zonally averaged Lagrangian mean flow. Clearly, the Eulerian mean flow is a bad predictor for particle behavior. We estimate the magnitude of this Lagrangian circulation to be less than 0.5 Sv.

Figure 19 shows the Lagrangian meridional velocity that indicates an equatorward flow on both sides of the equator. *Davis* (1995) demonstrated that particles will drift towards areas of higher variability and Figure 20 shows that in the interior the highest variance of meridional velocity is indeed along the equator.

This analysis shows that the Rossby waves generate a secondary circulation with eastward flow off the equator and westward flow at the equator. Tracers will converge towards the equator where they find the highest variance of meridional velocity. These effects are certainly not enough to explain the equatorial tracer distribution in the AAIW, but they should be taken into account in the analysis of the observations.

4. SUMMARY

The results of an OGCM were used to understand the observations of the AAIW in the tropical Atlantic. It is demonstrated that previous current and float observations in the intermediate layer of the tropical Atlantic should be interpreted as seasonal Rossby waves and not, as previously thought, as strong zonal currents. There are, however, very weak zonal flows along the equator which are due to a Rossby wave induced Stokes drift. This flow is to the west at the equator and to the east at 2°S/2°N, with speeds of the order of several mm/s.

Without the observations by *Schott et al.* (1998), one would be hard pressed to find any evidence for strong zonal jets at all, and we believe that the unfortunate timing of these observations (especially the two October measurements) led to the idea of strong zonal jets. Further confusion is probably caused by the zero crossing of the dominant mode of variability in the center of the AAIW (Figure 7). Because of the depth of this zero crossing, there is always AAIW flowing westward along the equator; depending on the season, the AAIW flows west above or below 700m depth (Figure 5). If one believes in intermediate jets, one can easily mistake the flow field as currents that change their depth over the course of a year. Thus, it is important to notice that the AAIW as a water mass is not necessarily related to the structure of the dynamical modes and that in a wave dominated environment the AAIW can flow in two different directions at the same time.

This study suggests that one should understand the observed velocity fields along the equatorial intermediate depths as the result of seasonal Rossby waves. It is not, however, a rigorous proof against the existence of intermediate currents. Rather, it shows that we need to increase the observational database in the tropical Atlantic before claiming to understand the tropical circulation.

Acknowledgements:
The authors benefitted from the helpful suggestions of Antonio Busalacchi, Glenn Flierl, Breck Owens, Mike Spall, and Gustavo Goni; Arne Biastoch is thanked for help with the open boundary conditions. The computations have been performed at the NCAR facilities in Colorado and this research was funded with NOAA grant Nr NA16GP1576 at MIT.

REFERENCES

Arhan, M., Mercier, H., Bourles, B., Gouriou, Y., 1998. Two hydrographic sections across the Atlantic at 7^o30N and 4^o30S . Deep-Sea Res. 45, 829–872.

Blanke, B., Arhan, M., Madec, G., Roche, S., 1999. Warm water paths in the equatorial Atlantic as diagnosed with a general circulation model. J.Phys.Oceanogr. 29, 2753–2768.

Boebel, O., Davis, R., Ollitrault, M., Peterson, R., Rich, P., Schmid, C., Zenk, W., 1999a. The intermediate depth circulation of the western south Atlantic. Geophys. Res. Let. 26, 3329–3332.

Boebel, O., Schmid, C., Zenk, W., 1999b. Kinematic elements of Antarctic Intermediate Water in the south Atlantic. Deep Sea Res. 46, 355–392.

Boening, C. W., Schott, F., 1993. Deep currents and the eastward salinity tongue in the equatorial Atlantic: Results from an eddy-resolving, primitive equation model. J.Geophys.Res. 98, 6991–6999.

Busalacchi, A. J., O'Brien, J., 1980. The seasonal variability in a model of the tropical Pacific. J.Phys.Oceanogr. 10, 1929–1951.

Busalacchi, A. J., Picault, J., 1983. The seasonal variability from a model of the tropical Atlantic. J.Phys.Oceanogr. 13, 1564–1588.

Davis, R., 1998. Preliminary results from directly measuring middepth circulation in the tropical and south Pacific. J.Geophys.Res 103, 24619–24639.

Hellerman, S., Rosenstein, M., 1983. Normal monthly wind stress over the world ocean with error estimates. J.Phys.Oceanogr. 13, 1093–1104.

Johns, W., Lee, T., Beardsley, R., Candela, J., Limeburner, R., Castro, B., 1998. Annual cycle and variability of the North Brazil Current. J.Phys.Oceanogr. 28, 103–128.

Li, X., Chang, P., Pacanowski, R., 1996. A wave-induced stirring mechanism in the mid-depth equatorial ocean. J.Mar.Res. 54, 487–520.

Liu, Z., Philander, S., 1995. How different wind stress patterns affect the tropical-subtropical circulations of the upper ocean. J.Phys.Oceanogr. 25, 449–462.

Oliger, O., Sundstrom, A., 1978. Theoretical and practical aspects of some initial boundary value problems in fluid dynamics. J. Appl. Math. 35, 419–446.

Philander, S., 1990. El Nino, La Nina and the Southern Oscillation. Academic Press.

Philander, S., Yamagata, T., Pacanowski, R., 1984. Unstable air-sea interaction in the tropics. J.Atmos.Sci. 41, 604–613.

Richardson, P., Schmitz, W., 1993. Deep cross-equatorial flow in the Atlantic measured with SOFAR floats. J.Geophys.Res 98, 8371–8387.

Rintoul, S., 1991. South Atlantic interbasin exchange. J.Geophys.Res. 96, 2675–2692.

Roemmich, D., 1983. The balance of geostrophic and Ekman transports in the tropcial Atlantic ocean. J.Phys.Oceanogr. 13, 1534–1539.

Schmid, C., Molinari, R., Garzoli, S., 2001. New observations of the intermediate depth circulation in the tropical Atlantic. J.Mar.Res. 59, 281–312.

Schmitz, W., McCartney, M., 1993. On the North Atlantic circulation. Rev. Geophys. 31.

Schmitz, W., Richardson, P., 1991. On the sources of the Florida Current. Deep Sea Research 38, S379–S408.

Schott, F., Fischer, J., Reppin, J., Send, U., 1993. On mean and seasonal currents and transports at the western boundary of the equatorial Atlantic. J.Geophys.Res. 98, 14353–14368.

Schott, F., Stramma, L., Fischer, J., 1998. Transports and pathways of the upper-layer circulation in the western tropical Atlantic. J.Phys.Oceanogr. 28, 1904–1928.

Spall, M., Robinson, A., 1989. A new open ocean, hybrid coordinate primitive equation model. Mathematics and Computers in Simulation 31, 241–269.

Stevens, D., 1990. On open boundary conditions for three dimensional primitive equation oceancirculation models. Geophys. Astrophys. Fluid Dynamics 51, 103–133.

Suga, T., Talley, L., 1995. Antarctic Intermediate Water circulation in the tropical and subtropical Atlantic. J.Geophys.Res 100, 13441–13453.

Weisberg, R., 1980. Equatorial waves during GATE and their relation to the mean zonal circulation. Deep-Sea Res., Supplement II 26, 179–198.

Weisberg, R., Horigan, A., 1981. Low-frequency variability in the equatorial Atlantic. J.Phys.Oceanogr. 11, 913–920.

Weisberg, R., Miller, L., Horigan, A., Knauss, J., 1980. Velocity observations in the equatorial thermocline during GATE. Deep-Sea Res., Supplement II 26, 217–248.